Pergamon

Geochimica et Cosmochimica Acta, Vol. 60, No. 20, pp. 3897–3912, 1996

0016-7037/96 $15.00 + .00

PII S0016-7037(96)00209-8

The size distribution of framboidal pyrite in modern sediments: An indicator of redox conditions

R. T. WILKIN, H. L. BARNES, and S. L. BRANTLEY

Ore Deposits Research Section, The Pennsylvania State University, University Park, PA 16802, USA

(*Received December* 28, 1995; *accepted in revised form June* 20, 1996)

Abstract—Pyrite framboids are densely packed, generally spherical aggregates of submicron-sized pyrite crystals. In this study, a survey was made of framboid size distributions in recently deposited sediments from euxinic (Black Sea; Framvaren Fjord, Norway; Pettaquamscutt River Estuary, Rhode Island, USA), dysoxic (Peru Margin), and oxic (Wallops Island, Virginia, USA; Great Salt Marsh, Delaware, USA) environments. Pyrite framboids in sediments of modern euxinic basins are on average smaller and less variable in size than those of sediments underlying dysoxic or oxic water columns. Down-core trends indicate framboid size distribution is a sediment property fixed very early during anoxic diagenesis, generally within the top few centimeters of burial. Size distributions in modern sediments are comparable with those in ancient sedimentary rocks, evidence that framboid size is preserved through advanced stages of diagenesis and lithification. It is proposed that where secondary pyrite growth is limited, as to preserve primary pyrite textures, framboid size distribution may be used to indicate whether fine-grained sedimentary rocks were deposited under oxic or anoxic conditions.

The Crystal Size Distribution Theory relates framboid size to growth time and rate. On the basis of this theory, the characteristic smaller sizes of framboids in sediments of modern euxinic basins reflect shorter average growth times relative to oxic or dysoxic environments. In euxinic environments, framboid nucleation and growth occurs within anoxic water columns, and growth times are, on average, shorter because of hydrodynamic effects than when framboid nucleation and growth occurs within anoxic sediment porewaters underlying oxic water columns. A maximum framboid growth time of 0.4 years is indicated for framboids forming in the water columns of euxinic basins.

1. INTRODUCTION

Bulk chemical and stable isotopic analyses of porewaters and solids are often used to follow chemical processes that occur during the diagenesis of modern anoxic sediments. These analyses are commonly applied to sedimentary rocks in attempts to reconstruct paleoenvironments (e.g., Leventhal, 1983; Raiswell et al., 1988; Jones and Manning, 1994). In contrast, relatively little attention has been given to the physical properties of authigenic minerals, for instance, mineral textures and size. With the notable exceptions of Sweeney and Kaplan (1973), Morse and Cornwell (1987), and Canfield et al. (1992), this is especially true in studies addressing the chemical and biochemical cycling of iron and sulfur in recent sediments. Bulk concentrations and sulfur isotopic compositions of several relevant solid and aqueous species are routinely measured, but typically the forms and distributions of iron sulfide minerals are not discussed. This investigation explores the dependence of the physical characteristics of sedimentary pyrite on genetic conditions.

Primary mineral textures in modern sediments should reveal information about original conditions of crystal growth and provide a means of directly comparing modern and ancient sedimentary environments. Pyrite is ubiquitous in modern anoxic sediments and is preserved in many ancient sedimentary rocks. Thus, characterization of the physical properties of pyrite in modern sediments deposited under unique depositional environments might serve as a tool to decipher the depositional environments of ancient sediments. Size is an easily measured physical property of a crystal or mineral aggregate and some quantitative information is available regarding pyrite size distributions in ancient sedimentary rocks (Love and Amstutz, 1966). In this paper, the size distributions of pyrite framboids in sediments from a variety of modern environments are reported and discussed in terms of a general model of crystal growth.

2. BACKGROUND

2.1. Morphology of Sedimentary Pyrite

Based on the petrographic descriptions of modern and ancient sediments given in Kalliokoski (1966), Love and Amstutz (1966), Sweeney and Kaplan (1973), Raiswell (1982), Hudson (1982), Schallreuter (1984), and Canfield and Raiswell (1991), sedimentary pyrite occurs as single or clustered framboids, single or clustered euhedral crystals, and replacements of organic matter. The relative proportion of these different textural types in a particular sediment is variable but all forms develop early during anoxic diagenesis, usually within the top few centimeters of a sediment column (Kaplan et al., 1963). Euhedral crystals and framboids are the dominant textural forms of pyrite in modern sediments as well as in ancient Phanerozoic, Proterozoic, and Archean sedimentary rocks (Love and Amstutz, 1966; Hallbauer, 1986). Therefore, both chemical (e.g., sulfur isotopic composition) and physical properties of these pyrite textures are promising indicators of past environmental conditions (e.g., Ohmoto et al., 1993).

The processes causing pyrite to have framboidal morphology, based on experimental and field studies, are generally thought to occur during the replacement of progressively

more S-rich phases: disordered mackinawite → ordered mackinawite (Fe_9S_8) → greigite (Fe_3S_4) → pyrite (FeS_2). The formation and growth of precursor ferrimagnetic greigite is a key stage of framboid development (e.g., Sweeney and Kaplan, 1973, Morse et al., 1987; Wilkin, 1995). It is puzzling that this sequence of reaction products rarely has been observed in natural environments; however, Nuhfer and Pavlovic (1979) have identified framboids composed of greigite in recent lacustrine sediments, and Roberts and Turner (1993) described magnetic pyrite framboids apparently containing residual greigite cores, implying that greigite is a precursor phase in the development of pyrite framboids.

2.2. Site of Framboid Formation

Several experimental studies have shown that greigite forms by a redox-dependent process requiring dissolved sulfide, ferrous iron, and an oxidant, such as oxygen (Berner, 1967), dissolved polysulfides (Wada, 1977; Dekkers and Schoonen, 1994), or elemental sulfur (Horiuchi et al., 1974). In nature, the maximum simultaneous production rates of these reactants are specifically limited to regions immediately subjacent to redox interfaces separating oxygen-bearing and hydrogen sulfide-bearing waters. Normally these redox interfaces are located just below, and within centimeters of, the sediment-water interface. However, in certain restricted coastal basins where mixing of water masses is limited, the rate of oxygen renewal to bottom waters can be less than the rates of organic matter oxidation; consequently, the redox interface can rise above the bottom sediments into the overlying water column. Indeed, in studies that specifically address the depth distribution of greigite, this mineral is present dominantly near the redox-interface, whether it be in the sediments (Cutter and Velinsky, 1988) or in the water column (Muramoto et al., 1991). Apparently greigite formation and framboid formation are linked to the oxic-anoxic transition.

The discovery of pyrite framboids suspended in the anoxic portion of the Black Sea was noted by Ross and Degens (1974). Degens et al. (1972) had previously shown scanning electron micrographs of pyrite framboids and sphalerite particles collected by filtration from the anoxic waters of Lake Kivu in the East African rift. Also, framboids have been found in suspended solids collected from the water column of Kau Bay (Middelburg et al., 1988) and the water columns of two meromictic lakes located in British Columbia, Canada (Perry and Pedersen, 1993). Concentrations of suspended pyrite in these lakes range from 50–500 nM; depth profiles of pyrite concentrations are complicated but do not suggest that the suspended pyrite is resuspended sedimentary material.

Pyrite framboids are common in the anoxic portion of the Black Sea as found by Muramoto et al. (1991) in a detailed study of sulfur, iron, and organic carbon fluxes through the Black Sea water column. The framboids are not found in polyframboidal clusters (Love, 1971) but are typically associated with biogenic particles. The average diameter of these framboids was reported to be 6 μm. The sulfur isotopic composition of particulate sulfides settling through the water column overlaps with that of dissolved sulfide immediately below the oxic-anoxic boundary but is enriched in ^{34}S by about 4‰ relative to deep-water dissolved sulfide. Based on these data, Muramoto et al. (1991) suggest that iron sulfide precipitation in the Black Sea occurs at the oxic-anoxic interface. A similar conclusion was reached by Lyons and Muramoto (1992) based on the sulfur isotopic composition of pyrite in the top 30 cm of laminated Black Sea sediments (Unit I). Again the isotopic composition of reduced sulfur buried in the sediments resembles dissolved sulfide at the chemocline rather than deep-water sulfide. Moreover, downcore constancy in the degree of pyritization implies that the pyrite formation is largely completed at or above the sediment-water interface (Lyons and Berner, 1992).

The formation of framboidal pyrite in the water column of the permanently anoxic Framvaren Fjord, Norway, has been documented by Skei (1988). In Framvaren Fjord, the anoxic-oxic boundary occurs within the photic zone at a depth of 20 m (Skei, 1983, 1988; Sælen et al., 1993). Skei (1988) identified suspended framboids at several water depths from the chemocline to the sediment-water interface at 180 m. The aggregates ranged in size from 3 to 10 μm and were composed of 0.3–0.7 μm microcrystals. Skei (1988) suggested that framboid formation at Framvaren Fjord occurs at the chemocline where metabolizeable organic matter (mainly purple photosynthetic bacteria), zero-valent sulfur, and reactive iron are abundant.

Framboid formation at the oxic-anoxic interface within sediments overlain by oxic water columns is indicated in several studies where sulfur isotopic values of pyrite framboids were found to be characteristically depleted in ^{34}S, suggesting that framboid growth occurred in porewaters open to the sediment-water interface so that free pathways were available for sulfate diffusion from overlying waters (Raiswell, 1982; Canfield et al., 1992). Canfield et al. (1992) found that framboidal pyrite is the dominant pyrite morphology during the earliest stage of diagenesis at the FOAM site in Long Island Sound, Connecticut, USA. These authors suggest that the early-formed pyrite develops from the most labile sources of iron in microenvironments experiencing high rates of sulfate reduction.

2.3. Framboid Nucleation and Growth

Crystal growth generally involves a diffusion step where solutes are transported to the mineral surface followed by a surface reaction that includes adsorption and inclusion into the crystal lattice (Nielsen, 1964; Stumm, 1992). Either of these steps may limit the rate of crystal growth. Although diffusion of molecular or ionic species to the mineral-water interface is often assumed to dominate, there is growing evidence showing that crystal growth may occur by the addition of very small (<100 nm) solute particles. In the later case, crystal growth is analogous to the process of colloid aggregation (e.g., Uyeda et al., 1973; Bogush and Zukoski, 1991).

The textures of framboids suggest that there is an initial stage of microcrystal nucleation and growth followed by microcrystal incorporation into framboids by aggregation (Taylor, 1982; Wilkin, 1995). Perhaps the most remarkable feature of framboids is that microcrystals in any one framboid invariably are uniformly sized (Love and Amstutz, 1966). This uniformity of size indicates that the microcrys-

Table 1. Locations and depositional environments of sediment samples discussed in text.

Location	Environment	Sample Type	References
Black Sea	deep stratified basin; euxinic (~2000 m)	Unit I, box core 53, station 103	Arthur *et al.* (1994)
Pettaquamscutt, RI (USA)	shallow stratified estuary; euxinic (~20 m)	surface sediments of Lower Basin	Gaines and Pilson (1972)
Framvaren Fjord (Norway)	shallow stratified fjord; euxinic (~200 m)	cores at 180 m (F1) and 100 m (F2)	Sælen *et al.* (1993)
Peru Margin	continental slope; upwelling zone; dysoxic	boxcore at 109 m	Suits *et al.* (1993)
Framvaren Fjord (Norway)	shallow stratified fjord; oxic (<18 m)	cores collected above (F3-15m) and at (F3-18m) redox interface	Sælen *et al.* (1993)
Wallops Island, VA (USA)	coastal zone, salt marsh; oxic	push cores low marsh	White *et al.* (1990)
Great Salt Marsh, DE (USA)	coastal zone, salt marsh; oxic	push cores high marsh	Lord and Church (1983)

tals in any one framboid nucleate simultaneously (as iron monosulfides) and growth is constant prior to aggregation. In this sense, the nucleation and the mean linear growth rate (G) of framboids discussed in following sections are related to the initiation and rate of aggregation of microcrystals, respectively, rather than to direct precipitation and growth of pyrite from solution. Microcrystal formation can be viewed in terms of nucleation and growth from solution; however, because of the difficulty in nucleating pyrite directly from solution (Schoonen and Barnes, 1991), it is likely that the microcrystal size apparent in pyrite framboids is remnant from iron monosulfide precursors.

3. SAMPLES AND ANALYTICAL METHODS

Sediment samples were collected from a variety of modern sites (Table 1) chosen to include a range of bottom-water oxygenation conditions, e.g., from oxic ($O_2 > 30\ \mu M$), dysoxic ($O_2 < 30\ \mu M$), and anoxic-sulfidic (i.e., euxinic) environments (see Arthur and Sageman, 1994). Detailed sedimentological and geochemical descriptions of these specific sites can be found in the references cited in Table 1. In general, the top ~30 cm of the sediment columns were sampled so that variations in the properties of pyrite could be studied as a function of depth below the sediment-water interface. Whenever possible sediment samples were stored in an evacuated desiccator to retard air oxidation of the constituent sulfide minerals.

Approximately 1–4 cm sections of the sediment cores were homogenized, gently dissaggregated using an agate mortar, and mixed in 3 cm-diameter molds with Spurr low-viscosity resin (E. F. Fullam, Inc.). After the resin had cured overnight at 70°C, the surfaces of the mounted samples were ground and polished (to 0.25 μm) with diamond pastes following standard techniques. This method does not preserve or allow for the study of original spatial relationships between crystals; however, sediment dissaggregation results in increased sediment surface area and consequent bonding between sediment and epoxy allowing for a superior polish. Approximately forty polished sections were examined using standard reflected-light microscopy, generally with a high-power (150×), oil-immersion objective lens and the size and morphology of each pyrite particle observed was recorded. The size of each pyrite particle was generally measured to $\pm 0.25\ \mu$m with a standard ocular graticule calibrated with a stage micrometer. Typically more than 100 particles were measured in each polished mount which resulted in stable size distribution statistics.

The amount of pyrite in the sediments was measured using a sequential extraction method. First a portion (~30 mg) of the sediment was treated with boiling 6 M HCl to remove acid-soluble sulfides and then with a 1 M $CrCl_2$ solution in 0.5 M HCl to remove mainly pyrite but some elemental sulfur (Canfield et al., 1986). The hydrogen sulfide gas evolved in these steps was quantitatively titrated with a sulfur coulometer (Atkin and Somerfield, 1994) to assess the total mass of pyrite per gram of sediment on a dry weight basis. The reproducibility of these measurements was always better than about 10% at the 2σ confidence level.

Pyrite concentrates were obtained for several samples by centrifuging about 5 g sediment charges in bromoform (4000 rpm, 30 min). The heavy fraction was separated, washed with acetone, and dried under a stream of N_2 gas. A small amount of this material was placed on a stub covered with a thin layer of silver paint and then coated with a thin layer of gold. A field emission scanning electron microscope (SEM; JEOL JSM-6300F) was used to examine the morphology and to measure the size distribution of pyrite particles. The centrifuge technique only yielded about 50–70% of the total expected pyrite based on the chemical extraction measurements described above suggesting that some pyrite is present in low-density aggregates not easily separated using centrifugation or that the pyrite concentration is overestimated using the chemical extraction procedure.

4. RESULTS

The concentration of pyrite in the sediments studied ranged from 42–452 μmol per gram of dry sediment, a range typical of modern sediments (e.g., Berner, 1984). In all samples, the majority of pyrite is present as framboids. For example, over 95% of pyrite from the Black Sea sediments is in the form of framboids, including both spherical and irregularly shaped aggregates of submicron-sized pyrite microcrystals. Examples of these morphologies are shown in Fig. 1. A similar tendency toward framboidal morphology is observed in samples from other euxinic environments (Framvaren Fjord, Pettaquamscutt River Estuary). Although pyrite framboids are the dominant textural form of pyrite in the sediments of dysoxic (Peru margin) and oxic environ-

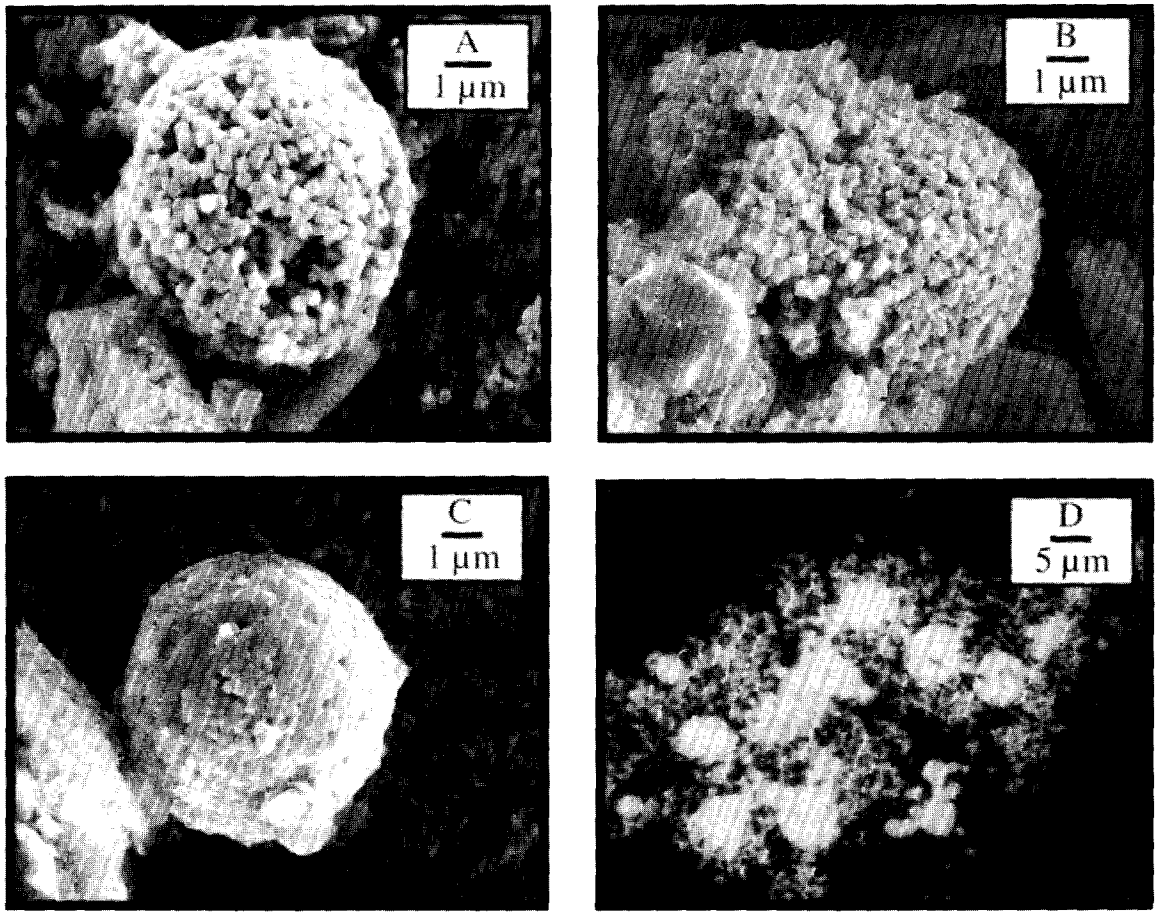

FIG. 1. SEM and reflected-light photomicrographs of pyrite framboids. (a) Spherical framboid from sediments of the Peru margin. (b) Framboid from sediments of the Great Salt Marsh. Note the irregular shape of the aggregate and that all the microcrystals (octahedrons) are equivalently sized. (c) "Infilled" framboid from sediments of the Peru margin. (d) Reflected-light photomicrograph of "infilled" pyrite spheres from Great Salt Marsh sediments; note euhedral overgrowths.

ments (Framvaren Fjord, Wallops Island, Great Salt Marsh), these sediments contain an increased proportion of euhedral forms and nondescript solid masses greater than 10 μm in size compared to the sediments of euxinic environments. Pyritized organic matter was not a significant component in any of the sediments discussed here.

Statistics of framboid size distributions, i.e., mean, standard deviation about the mean, and skewness, are listed in Table 2. The size distributions are represented graphically in histograms as a function of depth of burial for several selected sites in Fig. 2. The complete data set is included in Wilkin (1995). Because the polished surface of the mounts represents a random cut through an ensemble of nonuniform sized spheres, the measured size distributions are only an approximation of the true size distributions. In general, the true mean, for example, will be skewed to a slightly larger size relative to the mean computed from the measured distribution; however, this deviation is likely to be $<10\%$ (see Cashman and Marsh, 1988). A comparison between size distributions measured on the same sample using both optical microscopy and scanning electron microscopy is shown on a cumulative size distribution diagram (Fig. 3). The agreement between the two techniques is good, although the distribution obtained from optical microscopy is slightly skewed to larger size intervals. The histograms shown in Fig. 2 indicate that framboid diameter (D) is log-normally distributed. The difference between the untransformed and log-transformed statistics is small; for instance, geometric means are about 5% smaller than arithmetic means. For these reasons the measured distributions have not been transformed or corrected.

Descriptions of framboidal pyrite morphology and framboid size characteristics can be found in, among others, Love and Amstutz (1966), Kalliokoski and Cathles (1969), and Rickard (1970). In Table 3, compiled from literature sources are the average size and size range of pyrite framboids and their constituent microcrystals from both modern and ancient sediments. These data indicate that regardless of geologic age, pyrite framboids average 5 μm in diameter and are composed of crystals <1 μm in diameter, in general agreement with the size distribution measurements summarized in Table 2.

The number of microcrystals (N_M) in an idealized, spherical framboid composed of uniformly sized, spherical microcrystals in a cubic closest-packed (ccp) arrangement can be calculated knowing the framboid diameter (D), microcrystal

Table 2. Pyrite content and descriptive statistics of framboid size distributions from some modern and ancient sediments.

Sample	Depth (cm)	Pyrite (μmol/gm)	Mean (μm)	Standard deviation	Skewness	# framboids measured
Euxinic						
Black Sea	2	109	4.8	1.7	1.2	228
Black Sea	5	115	4.7	1.6	1.1	227
Black Sea	12	110	5.0	1.6	1.5	273
Black Sea	22	116	5.1	1.8	1.5	358
Black Sea	30	124	6.1	2.0	1.3	551
Pettaquamscutt	1-5	278	5.1	1.8	2.2	442
Framvaren (F1)[a]	1	42	4.8	1.7	1.1	109
Framvaren	3	44	5.2	2.0	1.2	127
Framvaren	5	42	5.0	1.6	0.9	70
Framvaren	6	120	4.4	1.5	1.0	108
Framvaren	8	157	5.0	1.8	1.6	109
Framvaren	10	109	4.3	1.4	1.2	109
Framvaren (F2)	7	80	4.9	1.4	0.6	228
Framvaren	9	134	5.4	2.0	1.4	110
Oxic-dysoxic						
Peru margin	2	150	6.5	2.9	2.0	271
Peru margin	6	178	6.1	2.6	3.1	278
Peru margin	10	176	6.4	3.0	2.1	231
Peru margin	14	167	5.7	2.9	2.6	192
Peru margin	16	178	6.7	3.5	1.6	170
Peru margin	30	110	7.0	3.2	1.7	352
Framvaren (F3-15m)	1	130	6.3	3.0	1.1	80
Framvaren	4	134	7.0	3.4	1.4	108
Framvaren	5	150	5.8	1.9	0.8	110
Framvaren	6	209	7.6	3.2	1.3	168
Framvaren	8	130	6.0	2.6	2.4	119
Framvaren	10	119	6.0	2.5	1.9	108
Framvaren (F3-18m)	7	452	5.8	3.2	2.0	235
Framvaren	8	455	8.1	4.6	2.0	162
Wallops Island	14	71	9.8	5.9	1.1	159
Wallops Island	40	284	8.1	4.1	0.8	132
Wallops Island	80	282	6.5	3.0	1.9	125
Wallops Island	120	98	6.9	2.8	1.7	145
Wallops Island	152	91	6.9	4.6	3.0	39
Great Salt Marsh	3	74	10.5	5.8	1.3	248
Great Salt Marsh	9	67	11.9	7.9	1.3	248
Great Salt Marsh	15	95	10.8	7.4	1.9	238
Great Salt Marsh	21	84	11.1	6.7	1.3	262
Great Salt Marsh	27	99	10.9	6.3	1.4	234
Great Salt Marsh	33	126	8.8	4.6	1.2	238
Ancient Sediments						
Chattanooga shale		nd	6.7	3.7	2.6	500
Rammelsberg shale		nd	5.9	2.1	1.0	581
Hartland shale		128	5.8	2.6	2.4	267

[a] - See Sælen et al. (1993) for sample locations at Framvaren Fjord.

diameter (d), and packing coefficient of the microcrystals (ϕ) with the equation:

$$N_M = \phi(D/d)^3. \quad (1)$$

Therefore, N_M can be determined from the slope on a plot of D vs. d because the ratio D/d is equivalent to the cube root of N_M/ϕ. Representative plots of D vs. d are shown in Fig. 4. Individual framboids from the sediments of the Black Sea and Great Salt Marsh typically contain fewer than about 20,000 microcrystals (see also Fig. 2 of Rickard, 1970). If the measured pyrite concentrations listed in Table 2 are partitioned into a population of average framboids (D = 5 μm), the total number of framboids per mass or volume of sediment can be estimated. The range of pyrite concentrations reported here (42–452 μmol/gm) corresponds to $10^{7.7 \pm 0.5}$ framboids per gram of sediment on a dry weight basis.

5. DISCUSSION

The framboid size distributions shown in Fig. 2 do not significantly change with depth in a particular sediment profile. The nonparametric Kolmogorov-Smirnov test, a particularly useful statistical test in comparing non-normally distributed variables (Davis, 1986), indicates that the down-core distributions are often indistinguishable at the 10% confi-

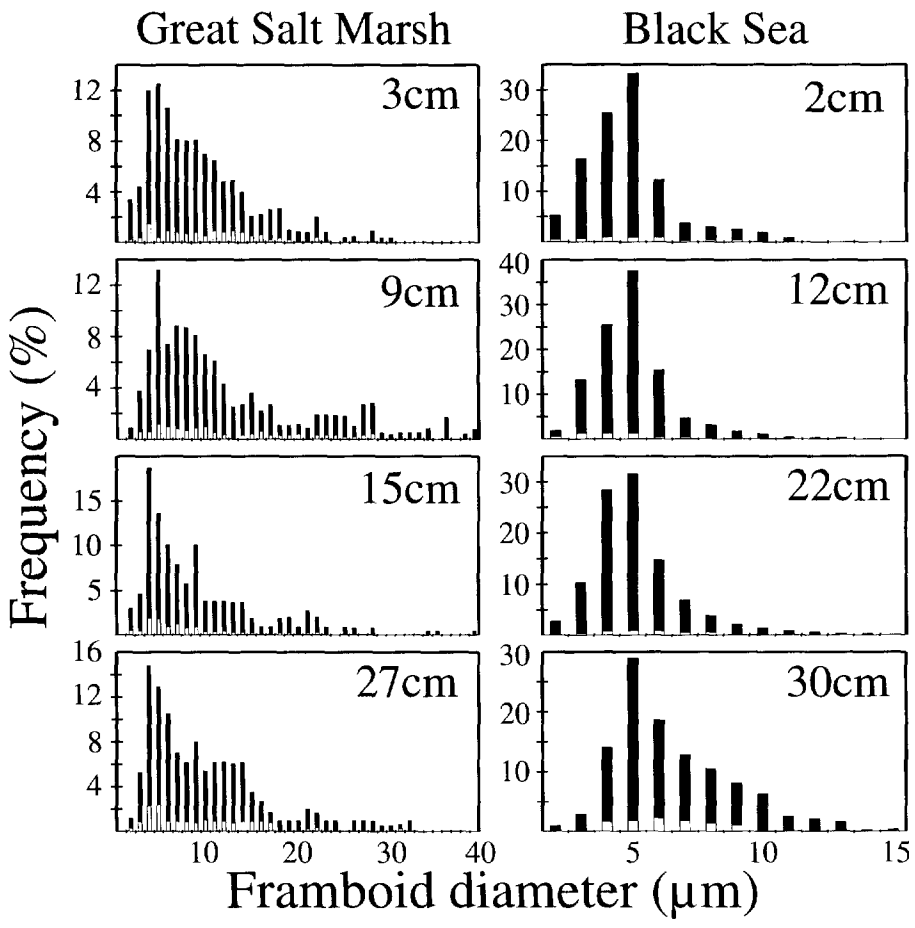

FIG. 2. Histograms showing the size frequency of pyrite framboids in sediments from the Great Salt Marsh (oxic) and Black Sea (euxinic) as a function of depth below the sediment-water interface. Unfilled bars indicate the frequency of framboids that show evidence of secondary growth or "infilling" (see Fig. 1).

dence level. The framboid size distribution with depth is generally constant in sediments overlain by either oxic or anoxic plus sulfidic water columns. Invariant pyrite concentration and size distribution with burial depth requires that framboid nucleation and growth, i.e., the addition of new microcrystals and the consequent increase in framboid diameter, does not continue with progressive burial. This cessation of framboid growth is consistent with the uniformity from rim to core of microcrystals in individual framboids, because nucleation events separated in time are unlikely to repeatedly produce equivalently sized microcrystals. The framboid size distribution, therefore, is a property that does not significantly change during early diagenesis. Moreover, the similarity of the size distributions reported here and those reported by Love and Amstutz (1966) for Devonian black shales indicates that framboid size distributions can persist over geologic time. Therefore, framboid size distribution may be a useful paleoenvironmental indicator.

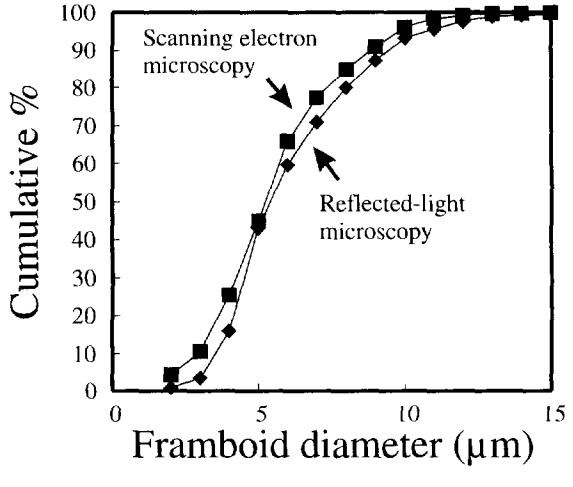

FIG. 3. Comparison of cumulative framboid size distributions from Black Sea sediments about 30 cm below the sediment-water interface. The size distributions were measured using reflected-light microscopy and scanning electron microscopy, respectively.

The percentage of framboids from Black Sea and Great Salt Marsh sediments with evidence of "infilling" or secondary pyrite formation in the interstices is shown in Fig. 2. Extreme cases of "infilling" destroy primary framboidal morphology due to the progressive formation of welded spheres of pyrite, euhedral overgrowths, pyritic masses, and large euhedral crystals (e.g., Love and Amstutz, 1966; Kalliokoski and Cathles, 1969; Ostwald and England; 1979; Sawlowicz, 1993). Pyrite framboids in the top several centi-

Table 3. Size characteristics of pyrite framboids.

Reference	Framboid diameter (μm)	Microcrystal diameter (μm)	Unit	Age
Ancient sediments				
Love and Zimmerman (1961)	1-15 (average: 5)	n.a.	Mt. Isa	Lower Proterozoic
Kalliokoski (1965)	(average: 6)	(average: 0.5)	Moscow	Devonian
Love and Amstutz (1966)	2-35 (average: 5-6)	<0.25-12 (most: <2.0)	Chattanooga	Devonian
Love and Amstutz (1966)	3-17 (average: 5-6)	<0.25-3 (most: <2.0)	Rammelsberg	Devonian
Kalliokoski and Cathles (1969)	4-25	0.5-5	Various	
Rickard (1970)	95%<40 (average: 4)	0.05-1	Tynagh	Mississippian
Love (1971)	5-50	n.a.	Denbigh Grit	Silurian
Swain (1986)	(average: 5)	(average: 1-2)	Liddel	Permian
Modern Sediments				
Vallentyne (1963)	3-32 (average: 8)	n.a.	Little Round Lake (Ontario)	
Schallreuter (1984)	3->30	0.1-1.5	Angola Basin	
Skei (1988)	3-10	0.3-0.7	Framvaren Fjord (Norway)	

n.a. = not available

meters of the Black Sea sediments show very limited infilling, though there does appear to be a slight increase of infilling with depth. Secondary growth is much more prevalent on pyrite framboids from the Great Salt Marsh (Fig. 2) where a positive correlation with depth is pronounced. For example, at 27 cm depth about 20% of the framboids show evidence of secondary pyrite growth. A similar pattern is observed to a lesser extent in the sediments from the Peru margin and Wallops Island. The framboid size distribution and morphology indicates a paragenesis of pyrite, where early formed framboids serve as sites for the continued growth of pyrite. The distribution of framboids showing secondary growth is similar to the original size distribution of Fig. 2 suggesting that secondary growth does not preferentially occur on either small or large framboids. Pyrite overgrowths tend to increase with depth in the sediments; thus, the longer pyrite surfaces are in contact with solutions containing appropriate solutes (e.g., Fe^{2+}, HS^-, S_x^{2-}), the more likely growth will continue. It is possible that this secondary growth is promoted in sediments where bioturbation acts to continuously remix deep and shallow sediments and porewaters.

5.1. Framboid Size Distribution as an Indicator of Depositional Environment

An important distinction has been made by Raiswell and Berner (1985) between *syngenetic* pyrite formed in the water columns of euxinic environments that settles to the sediment-water interface prior to burial and *diagenetic* pyrite formed in situ within the porewaters of anoxic marine sediments underlying oxic water columns. In either case, the initial amount of pyrite formed is controlled by the supplies of metabolizeable organic matter, of reactive iron, and of some weak oxidizing agent at the site of pyrite formation. This distinction between syngenetic and diagenetic sedimentary pyrite affects interpretations of the sulfur isotopic composition of pyrite (e.g., Muramoto et al., 1991; Sælen et al., 1993), bulk C/S values (e.g., Leventhal, 1983; 1995), and the degree of pyritization observed in ancient sediments (e.g., Raiswell et al., 1988).

The framboid size distributions presented here offer a useful means of discriminating between syngenetic and diagenetic sedimentary pyrites preserved in both modern sediments and ancient sedimentary rocks. In Fig. 5, the mean of the framboid size distributions for each locality is plotted against the corresponding size distribution standard deviation and skewness, respectively. Pyrite framboids contained in modern sediments underlying sulfidic water columns of the Black Sea, Framvaren Fjord, and Pettaquamscutt River Estuary are on average smaller and less variable in size than framboids from sediments underlying oxic or dysoxic water columns. The average mean framboid diameter ($\pm 1\sigma$) from sediments of modern euxinic environments and combined

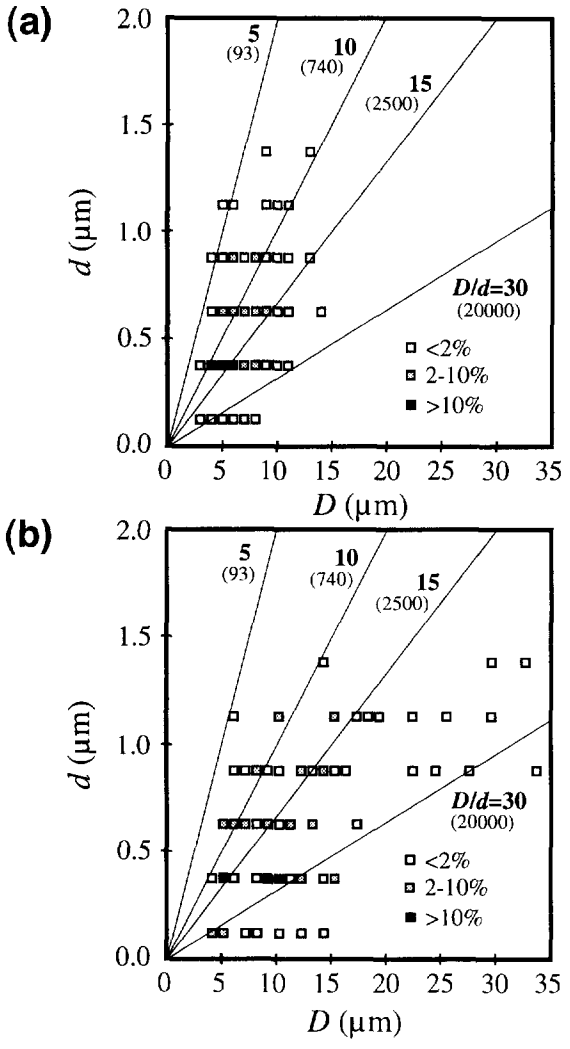

FIG. 4. Relationships between framboid diameters (D) and microcrystal diameters (d) in (a) Black Sea sediments (30 cm) and (b) Great Salt Marsh sediments (27 cm). The data points represent the scaled abundance (i.e., <2%, 2–10%, or >10%) of framboids with a particular diameter comprised of microcrystals with a particular diameter. The numbers in parentheses, corresponding to the given value of D/d in boldface type, are equal to the number of microcrystals present calculated with Eqn. 1 (ϕ = 0.74), e.g., all framboids with D/d = 5 contain ~93 microcrystals.

oxic and dysoxic environments are 5.0 ± 1.7 μm and 7.7 ± 4.1 μm, respectively. The positive linear relationship between these variables apparent in Fig. 5a is largely induced because of the dependence of the standard deviation on the mean. In Fig. 5a, the slope ($\sigma/\bar{X}$), i.e., the proportion of one standard deviation relative to the mean, indicates less variability of framboid size in euxinic environments compared to non-euxinic environments. For example, the ratio $\sigma/\bar{X}$ is relatively constant (0.34 ± 0.02) in framboid size distributions from euxinic sediments; whereas, $\sigma/\bar{X}$ is quite variable (0.55 ± 0.15) in non-euxinic sediments. The framboid size range is also indicative of depositional environment. In euxinic sediments, fewer than 4% of framboids are >10 μm; generally 10–50% of framboids in non-euxinic sediments are >10 μm. The same discrimination between environments can also be made with other moments of the size distributions, for example, the skewness (Fig. 5b).

Only one sample from Framvaren Fjord (F3-15-5) is misclassified based on the size distribution criteria (Fig. 5a). It is also possible that the chemocline at Framvaren Fjord has not been stationary over the past several decades. Also shown in Fig. 5 are size distribution data from two Devonian black shales and a Cretaceous laminated shale from the Western Interior seaway of North America. The size distribution data for the Devonian Chattanooga and Rammelsberg shales are taken directly from Love and Amstutz (1966, their Figs. 1 and 17). Framboid size distributions from the Rammelsberg and Chattanooga shales are similar to those from modern sediments deposited under euxinic and oxic or dysoxic conditions, respectively. Both of these shales, however, are characteristically laminated, contain abundant organic carbon, and are believed to have been deposited under stagnant water columns (Love and Amstutz, 1966). Thus, the classification of the Chattanooga pyrite as diagenetic is somewhat surprising, although the location of this sample is unknown. Based on iron-sulfur-organic carbon relationships, Dean and Arthur (1989) have suggested that bottom-water redox conditions in the Cretaceous seaway of North America varied from anoxic to slightly oxic which is consistent with the size distribution classification for the Hartland shale. Clearly multiple samples from any one environment are required to draw definitive conclusions using any proposed paleoenvironmental indicator. However, the overall similarity between the size distributions of framboids collected from modern sediments and shales deposited throughout the Phanerozoic, and the distinct clustering of distributions from modern environments demonstrates the utility of size distribution criteria as an indicator of ancient bottom-water redox conditions.

5.2. Application of the Crystal Size Distribution Theory

If all pyrite framboid nucleation in a particular volume of sediment or water column occurs simultaneously and growth of all nuclei proceeds at the same rate, then only one size of framboid will result. This size will be equal to the product of the mean linear growth rate (G) and the mean growth time (τ). The range of framboid sizes observed, therefore, is indicative of continuous framboid nucleation and growth during some time interval. A theoretical approach to understanding crystal size distributions (CSD) in chemical engineering systems was developed by Randolf and Larson (1988). This model has been applied to CSD in volcanic and metamorphic rocks (e.g., Cashman and Marsh, 1988; Cashman and Ferry, 1988), etch pit distributions on calcite and feldspar surfaces (e.g., MacInnis and Brantley, 1993; Brantley et al., 1993), and vesicle size distributions in lavas (Klug and Cashman, 1994).

The basis of the crystal size distribution theory (CSDT) is a population balance equation which describes the change in numbers and sizes of crystals in a system as a function of their residence times and as a function of loss and additions of crystals to the system. A population density parameter, n, is defined as the number of crystals in a given size range per unit volume of solution or:

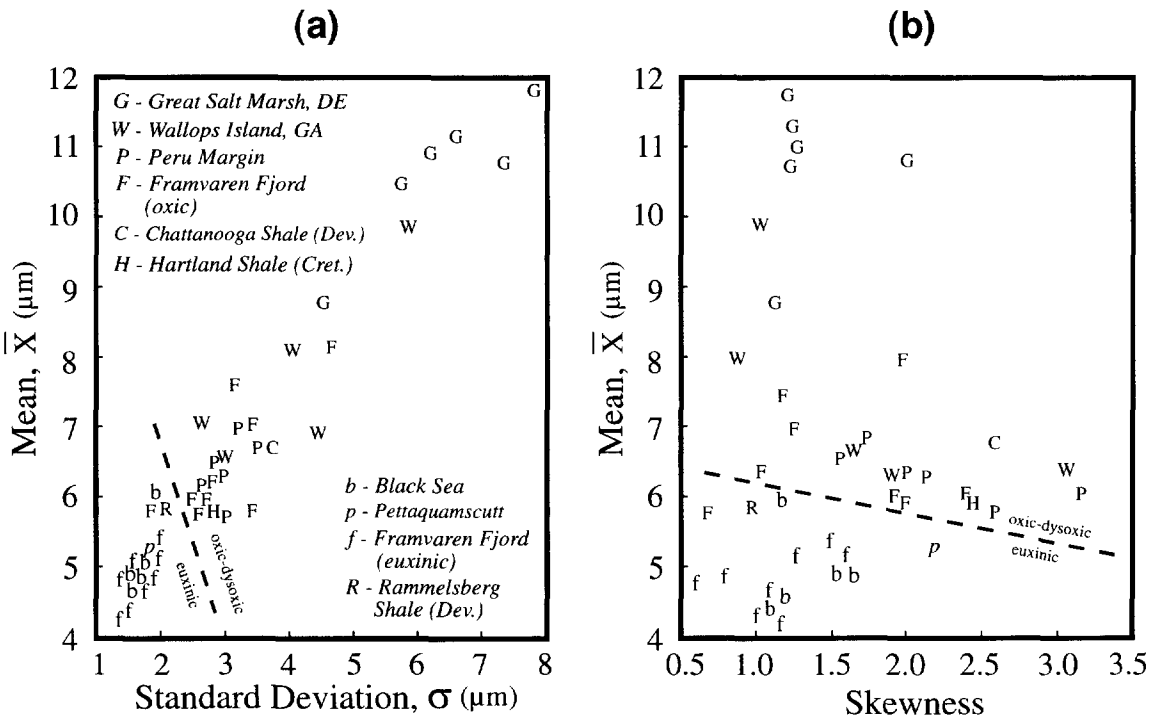

FIG. 5. (a) Plot of the mean versus the standard deviation of the framboid size distributions; (b) plot of the mean vs. the skewness of the framboid size distributions.

$$n = \Delta N/\Delta D \tag{2}$$

where N is the cumulative size distribution function and D is the crystal diameter. Thus, n is the slope on a cumulative size distribution diagram that can be constructed with data given in Fig. 2 (see Marsh, 1988). A population balance equation describing the number and size of pyrite framboids in a unit volume of solution is

(accumulation in ΔD)

$$= (\text{growth in-growth out}) + (\text{flux in-flux out}), \tag{3}$$

or based on a per volume accumulation:

$$(Vn_2 - Vn_1)\Delta D = (G_1Vn_1 - G_2Vn_2)\Delta t + (Q_in_i - Q_on_o)\Delta t\Delta D \tag{4}$$

where Q_in_i and Q_on_o represent the volume flux of particles with population densities n_i and n_o entering and leaving the crystallizing system, respectively. Rearranging terms, dividing by Δt and ΔD, and allowing both to approach zero yields the differential form of the population balance equation:

$$\frac{\partial(Vn)}{\partial t} + \frac{\partial(GVn)}{\partial D} = Q_in_i - Q_on_o. \tag{5}$$

Equation 5 represents the most general form of the population balance equation.

The general solution and application of Eqn. 5 requires certain restrictions on the crystallizing system (Randolf and Larson, 1988; Marsh, 1988). During continuous crystallization, the following assumptions and consequent simplifications of the population balance equation are made: (1) the influx of particles is much less than the outflux ($Q_in_i \ll Q_on_o$); physically this means that the crystallization is unseeded:

$$\frac{\partial(Vn)}{\partial t} + \frac{\partial(Gn)}{\partial D} + Q_on_o = 0, \tag{6}$$

(2) substituting the mean growth time ($\tau = V/Q_o$) and assuming crystallization occurs in an open system of constant volume:

$$\frac{\partial n}{\partial t} + \frac{\partial(Gn)}{\partial D} + \frac{n_o}{\tau} = 0, \tag{7}$$

(3) growth rate is independent of size (i.e., $G \neq f(D)$):

$$\frac{\partial n}{\partial t} + G\frac{\partial n}{\partial D} + \frac{n_o}{\tau} = 0, \tag{8}$$

and (4) crystallization occurs under steady state conditions ($\partial n/\partial t = 0$):

$$\frac{\partial n}{\partial D} + \frac{n_o}{G\tau} = 0. \tag{9}$$

The solution of this simplified population balance equation is

$$n = n^o e^{-(D/G\tau)} \tag{10}$$

or

$$\ln n = \ln n^{\circ} - D/G\tau \qquad (11)$$

where n° is defined as the nucleation density or the population density at the initiation of framboid nucleation. Before using this equation, discussion of the assumptions involved for pyrite-forming environments is given below.

Framboid formation in both euxinic and normal-marine environments is an example of a natural, unseeded, continuous crystallization process. Terrestrially derived particles of pyrite are unstable in oxic waters and do not constitute a flux to the chemocline of euxinic basins or the sediment-water interface underlying oxic water columns (Kaplan et al., 1963). A constant supply of pyrite-forming reactants are available at oxic-anoxic interfaces as follows. Dissolved sulfide is produced during the bacterially mediated reduction of dissolved sulfate. Ferrous iron is produced by either, or both, organic and inorganic reductive dissolution of ferric iron-bearing minerals, and weak oxidants such as dissolved polysulfides are available from both biochemical and chemical oxidation processes.

Kerrick et al. (1991) have pointed out that it is inappropriate to apply the CSD model to systems where crystals are not removed from the site of crystallization, i.e., where there is no Q_0 term in Eqn. 5. The steady state, framboid size distributions with burial depth (Fig. 2) demonstrate that framboids only form in restricted regions immediately subjacent to oxic-anoxic interfaces. Syngenetic framboids are removed by settling from the chemocline to the sediment-water interface; whereas, diagenetic framboids are buried, effectively removing them from the zone where framboid nucleation and growth occurs. Again note that although secondary pyrite growth may occur on framboids during early and late stages of diagenesis, this process does not, however, modify original framboid size distributions, except in extreme conditions where complete infilling and progressive overgrowths develop.

The assumption that growth rates do not change with crystal size (McCabe's law) is prevalent in chemical engineering applications where growth rates are primarily taken as functions only of supersaturation (Randolf and Larson, 1988). Because growth rates are also proportional to surface area and consequently D, size-independent growth is not a strictly valid assumption but is retained here as a first approximation. The effect of nonconstant G on framboid size distributions is discussed in a later section (see also Randolf and Larson, 1988, and Marsh, 1988). The steady state assumption ($\partial n/\partial t = 0$) means that crystallization proceeds from solutions that do not change with time, i.e., input nutrient and output removal fluxes are constant. This assumption is valid for continuous crystallization and not batch crystallizers where solution chemistry continually changes during the nucleation and growth processes. Although invariant crystallization conditions may not be realized in sedimentary processes, a steady state approximation is reasonable when integrating over extended periods of time by homogenizing 1–4 cm sections of sedimentary columns.

According to this model, if framboid size is governed by the assumptions outlined above, i.e., (1) crystallization is unseeded; (2) framboids are removed from the site of crys-

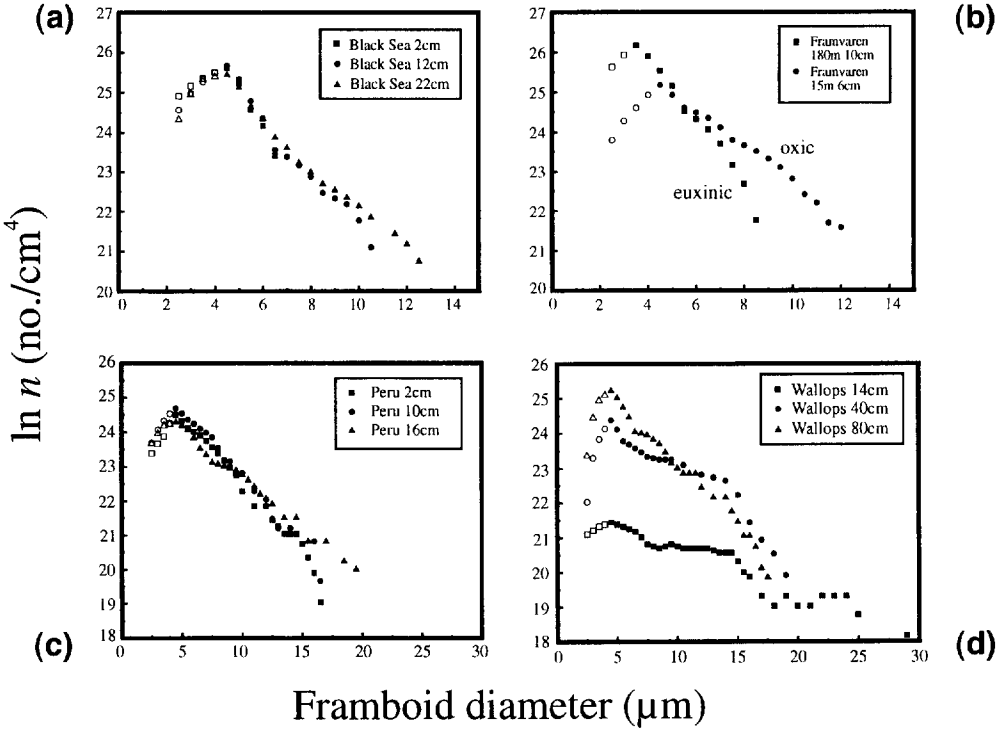

FIG. 6. Framboid size distribution plots of sediments from noted depths below the sediment-water interface of (a) the Black Sea, (b) Framvaren Fjord, (c) Peru margin, and (d) Wallops Island. Data points not used in the linear regressions are left open (see Table 4 for regression coefficients).

Table 4. Results of linear regression of framboid population density versus framboid diameter (± 1σ).

Sample	Depth (cm)	% pyrite as framboids	$\log_{10} N_{total}$ (no./cm^3)	ln n^o (no./cm^4)	$G\tau$ (μm)
Euxinic					
Black Sea	2	95	7.26	30.07 ±0.34	0.91 ±0.06
Black Sea	5	95	7.68	27.84 ±0.23	1.57 ±0.07
Black Sea	12	95	7.59	28.21 ±0.25	1.41 ±0.06
Black Sea	22	95	7.56	27.31 ±0.15	1.80 ±0.06
Black Sea	30	95	7.16	25.85 ±0.15	2.68 ±0.10
Pettaquamscutt	3	90	7.67	27.45 ±0.24	1.79 ±0.08
Framvaren	1	95	7.22	29.73 ±0.10	0.83 ±0.11
Framvaren	3	95	7.05	25.99 ±0.17	1.98 ±0.25
Framvaren	5	95	7.18	26.93 ±0.34	1.60 ±0.13
Framvaren	6	90	7.41	27.46 ±0.27	1.34 ±0.09
Framvaren	8	95	7.69	28.10 ±0.29	1.61 ±0.11
Framvaren	10	90	7.78	28.71 ±0.22	1.21 ±0.06
Framvaren	7	95	7.50	29.00 ±0.29	1.14 ±0.05
Framvaren	9	95	7.54	28.45 ±0.10	1.33 ±0.03
Oxic-dysoxic					
Peru margin	2	80	7.27	26.04 ±0.14	2.49 ±0.08
Peru margin	6	80	7.44	26.93 ±0.32	2.02 ±0.13
Peru margin	10	80	7.39	26.20 ±0.14	2.54 ±0.09
Peru margin	14	80	7.41	25.37 ±0.16	3.16 ±0.12
Peru margin	16	80	7.27	25.11 ±0.07	3.53 ±0.07
Peru margin	30	80	6.93	24.34 ±0.14	3.66 ±0.15
Framvaren	1	85	7.32	25.31 ±0.20	3.58 ±0.32
Framvaren	4	80	7.06	24.63 ±0.18	3.72 ±0.25
Framvaren	5	80	7.48	26.82 ±0.12	2.18 ±0.06
Framvaren	6	85	7.27	26.15 ±0.34	3.54 ±0.24
Framvaren	8	85	7.31	26.25 ±0.27	2.18 ±0.14
Framvaren	10	85	7.29	26.27 ±0.30	2.11 ±0.17
Framvaren	7	80	7.80	26.45 ±0.15	3.01 ±0.12
Framvaren	8	80	7.32	25.54 ±0.15	3.27 ±0.16
Wallops Island	14	75	6.29	21.69 ±0.10	7.66 ±0.39
Wallops Island	40	70	7.29	25.92 ±0.21	4.04 ±0.29
Wallops Island	80	70	7.54	26.20 ±0.13	2.75 ±0.09
Wallops Island	120	70	7.05	25.44 ±0.20	2.53 ±0.10
Wallops Island	152	70	6.98	25.57 ±0.31	2.98 ±0.13
Great Salt Marsh	3	75	6.28	22.18 ±0.14	5.79 ±0.32
Great Salt Marsh	9	70	5.81	20.44 ±0.12	8.54 ±0.42
Great Salt Marsh	15	65	6.18	21.33 ±0.15	7.30 ±1.24
Great Salt Marsh	21	65	6.41	21.80 ±0.08	8.20 ±0.36
Great Salt Marsh	27	65	6.27	22.14 ±0.08	5.16 ±0.17
Great Salt Marsh	33	65	6.78	21.50 ±0.11	7.91 ±0.40
Ancient sediments					
Chattanooga shale					3.69 ±0.20
Rammelsberg shale					1.72 ±0.06
Hartland shale		75			2.10 ±0.10

tallization; (3) reactant solutes are supplied at a constant rate; and (4) G is not a function of framboid size (D), then a plot of ln n vs. D will yield linear trends with slopes of $1/G\tau$ and intercepts of n°. Thus, if either G or τ are known the other may be computed. The population density, n, can be determined by numerical evaluation of the slope on cumulative size distribution diagrams (Wilkin and Barnes, 1994; Wilkin, 1995). Representative plots of the population density against framboid diameter are shown in Fig. 6. The calculated intercepts and slopes of all samples are given in Table 4. Only the negatively correlated, linear portions of the data in Fig. 6 have been utilized to determine the slopes and intercepts in Table 4.

Each of the plots in Fig. 6 shows a peak or a maximum in the population density near 5 μm corresponding to the mode of the histograms in Fig. 2. Some authors have argued that bell-shaped curves result from Ostwald ripening, by which matter is transferred from small particles to large particles (Randolf and Larson, 1988; Cashman and Ferry, 1988). The ripening process is driven by solubility differences between nonuniform-sized particles of a precipitate which establishes concentration gradients between smaller and larger particles. However, because anoxic and sulfidic waters are typically close to saturation with iron monosulfides but vastly supersaturated with respect to pyrite (e.g., Raiswell et al., 1993), the reaction affinity is such that there is no driving force for pyrite dissolution or the ripening process. Furthermore, we see no evidence for the selective

dissolution of framboids in the 2–5 μm size range; the exterior surfaces of the smallest framboids do not appear to be corroded as evidenced by the constancy of microcrystal diameters from aggregate rim to core. Kerrick et al. (1991) have shown that bell-shaped curves can be generated also by varying the rates of nucleation and growth during batch crystallization. The bell-shaped curves shown here (Fig. 6) might also be explained by the preferential removal of small framboids from the population by aggregation, reducing the population density of framboids at small sizes. This interpretation requires that the bell-shaped nature of the curves be a consequence of the framboid growth process and is consistent with the fact that the size corresponding to the maximum population density is essentially invariant in samples collected from different contemporary environments and from different geologic time periods. It is also possible that the abundance of the smallest framboids is underestimated by optical microscopy.

In sediments from the Black Sea and Peru margin, framboid size distributions do not vary with burial depth (Fig. 6). The constancy of size distribution indicates that factors controlling framboid size remain constant with time and reinforces the validity of the steady state approximation discussed previously. A steady state, however, is not apparent from the size distributions in salt marsh sediments from Wallops Island and the Great Salt Marsh (Fig. 6; Table 4). It is perhaps reasonable that salt marsh environments provide dynamic conditions for framboid growth because of generally high rates of sulfate reduction in such environments, and because the surfaces of salt marsh sediments are exposed to the atmosphere and the rhizosphere of marsh grasses can oxidize sediments at depth (Luther et al., 1982). Thus, dissolved hydrogen sulfide can readily be partially oxidized to polysulfides (S_x^{2-}) or other sulfur species with intermediate oxidation states at a range of horizons below the oxic-anoxic interface. These factors lead to dynamic cycling of iron and sulfur in space and time that may result in nonsteady-state pyrite growth conditions and more complicated framboid size distributions.

It is commonly assumed in applications of the CSD model that growth rates do not vary with time or grain size. This assumption in part simplifies the general population balance equation by allowing G in the second term of Eqn. 7 to be taken outside of the derivative and treated as a constant. Randolf and Larson (1988) have evaluated more general models of crystal growth where G is allowed to vary with crystal size. They find that the resulting plots of ln n vs. crystal size show pronounced curvature. For example, concave-upward trends are apparent when growth rates increase with grain diameter, whereas concave-downward trends are produced when growth rates decrease with grain diameter. With the exception of the salt marsh sediment from Wallops Island, the absence of pronounced curvature in the plots in Fig. 6 suggests that size-dependent growth is not a major factor controlling framboid size distribution in Black Sea, Framvaren Fjord, or Peru margin sediments.

The principles of the CSD theory have been extended to the process of particle aggregation in aqueous solutions by Hoyt (1978) and Randolf and Larson (1988). In their treatments, the population balance equation (Eqn. 4) is modified to include the nucleation and growth of primary crystallites (microcrystals) and the consequent incorporation of these crystallites into aggregates (framboids). The relationship between framboid diameter and microcrystal diameter de-

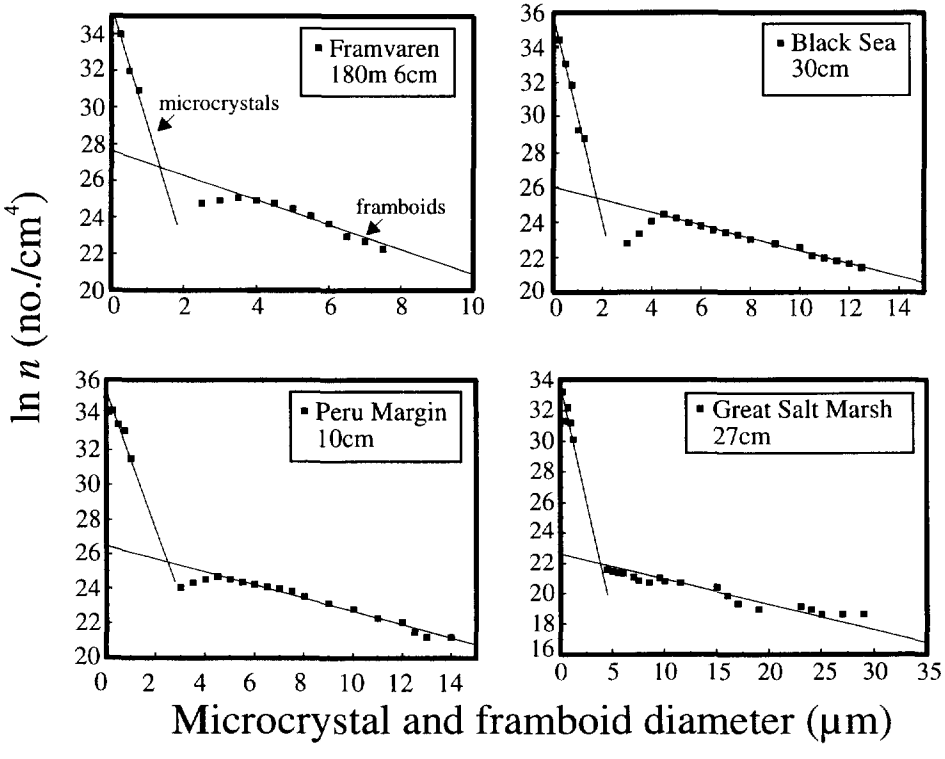

FIG. 7. Microcrystal and framboid size distribution plots of four samples (see Table 5 for regression coefficients).

Table 5. Results of linear regression of microcrystal population density versus microcrystal diameter (± 1σ).

Sample	$(\ln n^0)_M$ (no./cm^4)	$(G\tau)_M$ (μm)	$(G\tau)_F$ (μm)	$(G\tau)_F/(G\tau)_M$
Euxinic				
Black Sea (30 cm)	35.99 ±0.52	0.17 ±0.02	2.68 ±0.10	15.8
Framvaren (6 cm)	35.35 ±0.58	0.16 ±0.02	1.34 ±0.09	8.4
Oxic-dysoxic				
Peru Margin (10 cm)	35.23 ±0.49	0.29 ±0.05	2.54 ±0.09	8.8
Great Salt Marsh (27 cm)	33.55 ±0.73	0.39 ±0.10	5.16 ±0.17	13.2

scribed in Eqn. 1 is used to sum the total number of microcrystals in a sample and to calculate the microcrystal population density function (Wilkin, 1995). Examples of the size distributions of both microcrystals and framboids are shown in Fig. 7 and regression coefficients are given in Table 5. The significantly different slopes shown on Fig. 7 further indicate that the factors controlling growth are different between microcrystals and framboids. The slopes of the microcrystal data are steeper than for the framboidal aggregates suggesting that the microcrystals grow more slowly than framboids or they grow for a shorter period of time at a faster rate. In the four samples shown in Table 5 the values of $G\tau$ of the framboids are about an order of magnitude greater than the $G\tau$ of the microcrystals. Thus, if microcrystals and framboids grow over the same time period, i.e., $\tau_M = \tau_F$, the framboid growth rate is about 10× that of the microcrystals.

5.3. Geologic Implications of the CSD Model

In industrial applications, the mean growth time (τ) is known; therefore, the CSD model allows the calculation of G. For the system described here, neither G or τ are known with certainty. Practical application of this model, therefore, requires approximations of either growth rates or growth times. Sediments collected from the Black Sea, Pettaquamscutt River Estuary, and the anoxic portion of Framvaren Fjord have framboid size distributions that yield $G\tau$ values or average sizes of 1.8 μm (±0.9). Note that this size is slightly smaller than the average framboid diameter from these environments (ca. 5 μm) because the slopes on Fig. 6, from which the $G\tau$ parameter is calculated, were determined using the linear portion of the size data and do not take into account the reduced population of framboids in the size range below about 5 μm. The average value of $G\tau$ in samples from the Peru margin, Wallops Island, Great Salt Marsh, all (dys)oxic, and the oxic portion of Framvaren Fjord is 5.3 μm (±3.2). The relatively small variability of $G\tau$ values or average framboid size in samples from euxinic environments suggests that the factors affecting growth rates and growth times of framboids in such environments do not vary much with time; however, more variability in growth parameters is suggested, based on considerable variability in $G\tau$ values, where framboid growth occurs within sedimentary porewaters.

The contrast in framboid size as a function of the two growth environments is shown in Fig. 6b. Both of these samples are from Framvaren Fjord, but they were collected from different sides of the oxic-anoxic boundary. The sample collected from the deep part of the basin has $G\tau$ = 1.2 μm, whereas the sample collected from sediments above the oxic-anoxic interface has $G\tau$ = 3.5 μm. If it is assumed that the framboid growth rate was the same in each of these samples, then the differences in the values of $G\tau$ reflect differences of average growth times. Thus, assuming constant G, the average growth time of diagenetic framboids is about three times that of syngenetic framboids at Framvaren Fjord. The size distribution criteria discussed previously, therefore, may be the result of differences in the growth time between framboids formed in euxinic and non-euxinic environments, respectively.

Based on settling times determined from Stokes' law, Skei (1988) and Muramoto et al. (1991) suggested short residence times for framboids suspended in the water columns of Framvaren Fjord and the Black Sea. In Fig. 8, the terminal settling velocity of framboids in still water, predicted with Stokes' law, is shown as a function of framboid diameter. The bulk framboid density is calculated assuming a cubic close-packing of microcrystals and interstitial void space filled with water. A narrow size distribution of framboids in

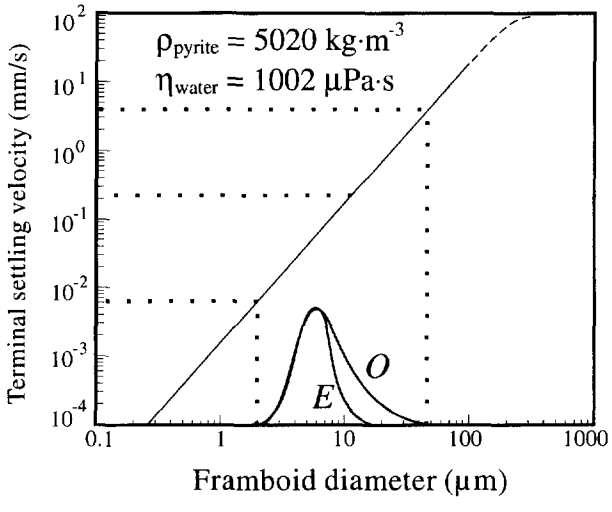

FIG. 8. Theoretical settling velocities of framboids in still water vs. their diameter computed with Stokes' law. Distributions E and O are representative of those from the sediments of euxinic and oxic environments, respectively.

euxinic sediments is not surprising because settling velocities vary as the square of the particle diameter and the first power of the buoyant density. The settling rate and overall residence time of framboids in euxinic water columns is a complicated variable that will depend on gravity, density differences, thermal motions, turbulence, and other particle-particle interactions.

Constraints on growth rates of diagenetic framboids can also be made by considering sedimentation rates. For example, the maximum framboid diameter in sediments from the Peru margin is about 25 μm. The pyrite concentration profile from the Peru margin core suggests that pyrite formation was completed within the top 2 cm of the sediment column (Table 2; see also Suits et al., 1993). Froelich et al. (1988) give a sedimentation rate for this region of the Peru margin of 0.3 cm/y. If the growth of the largest framboid takes place during the entire time interval in which 2 cm of sediments accumulate, a maximum growth time of about 7 years is indicated giving a minimum growth rate of this large framboid of about 4 μm/y. Again assuming constant framboid growth rates, and taking an average value of $G\tau$ from the Black Sea sediments of 1.7 μm, a maximum growth time of 0.4 years is indicated for framboids formed in the Black Sea water column.

6. SUMMARY AND CONCLUSIONS

The size distributions were measured of pyrite framboids and their microcrystals in sediments underlying several modern anoxic and oxic water columns. Framboid size distributions were found generally not to vary as a function of burial depth over the top ~30 cm of sediment cores collected from euxinic and normal-marine sedimentary environments. The independence of size with burial depth indicates that framboid growth does not continue with progressive burial, but rather is restricted to the earliest stages of anoxic diagenesis. The framboid size distributions in modern sediments reported here are comparable to those in two Devonian black shales previously described by Love and Amstutz (1966). Framboid size distribution is a representative primary property of anoxic sediments that can be preserved through geologic time.

Framboids formed in the water columns of modern euxinic basins (syngenetic) are on average smaller and less variable in size than those formed in modern sediments underlying oxic water columns (diagenetic). Therefore, basic statistical properties of framboid size distributions measured from ancient sedimentary rocks can be used to indicate whether sediment deposition occurred under sulfidic or oxic water columns.

Framboid size may largely be controlled by the residence time near the oxic-anoxic boundary. Framboid growth times, because of the hydrodynamic instability of pyrite particles in suspension, are shorter in euxinic environments than oxic environments. The Crystal Size Distribution Theory (Randolf and Larson, 1988) offers a method to estimate framboid growth rates and growth times from the size distribution data. For example, framboid size distributions in sediments collected both below and above the chemocline at Framvaren Fjord suggest that diagenetic framboids grow about three times longer than syngenetic framboids at Framvaren Fjord. This conclusion assumes that framboid growth rates are comparable in both types of environments. Estimates of framboid growth rates based on sedimentation rates suggest that framboid growth times in the water columns of euxinic basins are less than 0.4 years.

A common paragenetic sequence of pyrite morphologies from early framboidal aggregates, to progressively infilled aggregates, to euhedral overgrowths was observed in all environments discussed here. A significant fraction of euhedral grains within sediments may form during both early and late stages of burial diagenesis by secondary pyrite growth on previously formed framboid surfaces.

Acknowledgments—This paper represents part of the senior author's Ph.D. dissertation at The Pennsylvania State University. The research was supported by the National Science Foundation (EAR-8903750) and by the Ore Deposits Research Section of The Pennsylvania State University. Our gratitude is extended to M. Arthur, G. Sælen, N. Suits, and T. White for providing some of the sediment samples used in this study. The manuscript benefited from helpful reviews by R. Raiswell, M. Schoonen, R. Sweeney, and E. Merino.

Editorial handling: E. Merino

REFERENCES

Arthur M. A. and Sageman B. B. (1994) Marine black shales: Depositional mechanisms and environments of ancient deposits. *Ann. Rev. Earth Planet. Sci.* **22,** 499–551.

Arthur M. A., Dean W. E., Neff E. D., Hay B. J., King J., and Jones G. (1994) Varve calibrated records of carbonate and organic carbon accumulation over the last 2000 years in the Black Sea. *Global Biogeochem. Cycles* **8,** 195–217.

Atkin B. P. and Somerfield C. (1994) The determination of total sulphur in geological materials by coulometric titration. *Chem. Geol.* **111,** 131–134.

Berner R. A. (1967) Thermodynamic stability of sedimentary iron sulfides. *Amer. J. Sci.* **265,** 773–785.

Berner R. A. (1984) Sedimentary pyrite formation: An update. *Geochim. Cosmochim. Acta* **48,** 605–615.

Bogush G. H. and Zukoski C. F. (1991) Uniform silica particle precipitation: An aggregative growth model. *J. Colloid Interface Sci.* **142,** 19–34.

Brantley S. L., Blai A. C., Cremeens D. L., MacInnis I., and Darmody R. G. (1993) Natural etching rates of feldspar and hornblende. *Aquat. Sci.* **55,** 262–272.

Canfield D. E. and Raiswell R. (1991) Pyrite formation and fossil preservation. In *Taphonomy: Releasing the Data Locked in the Fossil Record* (ed. P. A. Allison and D. E. G. Briggs), Vol. 9 of *Topics in Geobiology,* Chap. 7, pp. 337–387. Plenum Press.

Canfield D. E., Raiswell R., Westrich J. T., Reaves C. M., and Berner R. A. (1986) The use of chromium reduction in the analysis of reduced inorganic sulfur in sediments and shales. *Chem. Geol.* **54,** 149–155.

Canfield D. E., Raiswell R., and Bottrell S. (1992) The reactivity of sedimentary iron minerals towards sulfide. *Amer. J. Sci.* **292,** 659–683.

Cashman K. V. and Ferry J. M. (1988) Crystal size distribution (CSD) in rocks and the kinetics and dynamics of crystallization III: Metamorphic crystallization. *Contrib. Mineral. Petrol.* **99,** 401–415.

Cashman K. V. and Marsh B. (1988) Crystal size distribution (CSD) in rocks and the kinetics and dynamics of crystallization II: Makaopuhil lava lake. *Contrib. Mineral. Petrol.* **99,** 292–305.

Cutter G. A. and Velinsky D. J. (1988) Temporal variations of sedimentary sulfur in a Delaware salt marsh. *Mar. Chem.* **23,** 311–327.

Davis J. C. (1986) *Statistics and Data Analysis in Geology*. Wiley.
Dean W. E. and Arthur M. A. (1989) Iron-sulfur-carbon relationships in organic-carbon-rich sequences I: Cretaceous western interior seaway. *Amer. J. Sci.* **289,** 708–743.
Degens E. T., Okada H., Honjo S., and Hathaway J. C. (1972) Microcrystalline sphalerite in resin globules suspended in Lake Kivu, East Africa. *Miner. Deposita* **7,** 1–12.
Dekkers M. J. and Schoonen M. A. A. (1994) An electrokinetic study of synthetic greigite and pyrrhotite. *Geochim. Cosmochim. Acta* **58,** 4147–4153.
Froelich P. N. et al.(1988) Early diagenesis of organic matter in Peru continental margin sediments: Phosphorite precipitation. *Mar. Geol.* **80,** 309–343.
Gaines A. G. and Pilson M. E. Q. (1972) Anoxic water in the Pettaquamscutt River. *Limnol. Oceanogr.* **17,** 42–49.
Hallbauer D. K. (1986) The mineralogy and geochemistry of Witwatersrand pyrite, gold, uranium, and carbonaceous matter. In *Mineral Deposits of Southern Africa* (ed. C. R. Anhaeusser and S. Maske), pp. 731–752. Geological Society of South Africa.
Horiuchi S., Wada H., and Moori T. (1974) Morphology and imperfection of hydrothermally synthesized greigite (Fe_3S_4). *J. Cryst. Growth* **24,** 624–626.
Hoyt R. C. (1978) Precipitation kinetics of a continuous precipitator, with applications to the precipitation of ammonium polyuranate. Ph.D. dissertation, Iowa State Univ.
Hudson J. D. (1982) Pyrite in ammonite-bearing shales from the Jurassic of England and Germany. *Sedimentology* **29,** 639–667.
Jones B. and Manning D. A. C. (1994) Comparison of geochemical indices used for the interpretation of paleoredox conditions in ancient mudstones. *Chem. Geol.* **111,** 111–129.
Kalliokoski J. (1965) Framboids: colloid-crystals of pyrite. *Econ. Geol.* **60,** 1562.
Kalliokoski J. (1966) Diagenetic pyritization in three sedimentary rocks. *Econ. Geol.* **61,** 872–885.
Kalliokoski J. and Cathles L. (1969) Morphology, mode of formation, and diagenetic changes in framboids. *Bull. Geol. Soc. Finland* **41,** 153–133.
Kaplan I. R., Emery K. O., and Rittenberg S. C. (1963) The distribution and isotopic abundance of sulphur in recent marine sediments off southern California. *Geochim. Cosmochim. Acta* **27,** 297–331.
Kerrick D. M., Lasaga A. C., and Raeburn S. P. (1991) Kinetics of heterogeneous reactions. In *Contact Metamorphism* (ed. D. M. Kerrick); *Rev. Mineral.* **26,** 583–671
Klug C. and Cashman K. (1994) Vesiculation of May 18, 1980, Mount St. Helen's magma. *Geology* **22,** 468–472.
Leventhal J. S. (1983) An interpretation of carbon and sulfur relationships in Black Sea sediments as indicators of environments of deposition. *Geochim. Cosmochim. Acta* **47,** 133–137.
Leventhal J. S. (1995) Carbon-sulfur plots to show diagenetic and epigenetic sulfidation in sediments. *Geochim. Cosmochim. Acta* **59,** 1207–1211.
Lord C. J., III, and Church T. M. (1983) The geochemistry of salt marshes: Sedimentary ion diffusion, sulfate reduction, and pyritization. *Geochim. Cosmochim. Acta* **47,** 1381–1391.
Love L. G. (1971) Early diagenetic polyframboidal pyrite, primary and redeposited, from the Wenlockian Denbigh Grit Group, Conway, North Wales, U.K. *J. Sediment. Petrol.* **41,** 1038–1044.
Love L. G. and Amstutz G. C. (1966) Review of microscopic pyrite from the Devonian Chattanooga Shale and Rammelsberg Banderz. *Fortschr. Mineral.* **43,** 273–309.
Love L. G. and Zimmerman D. O. (1961) Bedded pyrite and microorganisms from the Mount Isa shale. *Econ. Geol.* **56,** 873–896.
Luther G. W., III, Giblin A., Howarth R. W., and Ryans R. A. (1982) Pyrite and oxidized iron mineral phases formed from pyrite oxidation in salt marsh and estuarine sediments. *Geochim. Cosmochim. Acta* **46,** 2665–2669.
Lyons T. W. and Berner R. A. (1992) Carbon-sulfur-iron systematics of the uppermost deep-water sediments of the Black Sea. *Chem. Geol.* **99,** 1–27.
Lyons T. W. and Muramoto J. A. (1992) Water-column pyrite formation in the modern Black Sea: Sulfur isotopic constraints. *Geol. Soc. Amer. Abstr. Prog.* **24,** A168 (abstr.).
MacInnis I. N. and Brantley S. L. (1993) Development of etch pit size distributions on dissolving minerals. *Chem. Geol.* **105,** 31–49.
Marsh B. D. (1988) Crystal size distribution (CSD) in rocks and the kinetics and dynamics of crystallization I: Theory. *Contrib. Mineral. Petrol.* **99,** 277–291.
Middelburg J. J., De Lange G. J., van der Sloot H. A., Emburg P. R., and Sophiah S. (1988) Particulate manganese and iron framboids in Kau Bay, Halmahera (Eastern Indonesia). *Mar. Chem.* **23,** 353–364.
Morse J. W. and Cornwell J. C. (1987) Analysis and distribution of iron sulfide minerals in recent anoxic marine sediments. *Mar. Chem.* **22,** 55–69.
Morse J. W., Millero F. J., Cornwell J. C., and Rickard D. (1987) The chemistry of the hydrogen sulfide and iron sulfide systems in natural waters. *Earth Sci. Rev.* **24,** 1–42.
Muramoto J. A., Honjo S., Fry B., Hay B. J., Howarth R. W., and Cisne J. L. (1991) Sulfur, iron and organic carbon fluxes in the Black Sea: sulfur isotopic evidence for origin of sulfur fluxes. *Deep-Sea Res.* **38,** S1151–S1187.
Nielsen A. E. (1964) *Kinetics of Precipitation*. Pergamon Press.
Nuhfer E. B. and Pavlovic A. S. (1979) Association of kaolinite with pyritic framboids. *J. Sediment. Petrol.* **49,** 321–323.
Ohmoto H., Kakegawa T., and Lowe D. R. (1993) 3.4-billion-year-old biogenic pyrites from Barberton, South Africa: sulfur isotope evidence. *Science* **262,** 555–557.
Ostwald J. and England B. M. (1979) The relationship between euhedral and framboidal pyrite in base-metal sulfide ores. *Mineral. Mag.* **43,** 297–300.
Perry K. A. and Pedersen T. F. (1993) Sulphur speciation and pyrite formation in meromictic ex-fjords. *Geochim. Cosmochim. Acta* **57,** 4405–4418.
Raiswell R. (1982) Pyrite texture, isotopic composition and availability of iron. *Amer. J. Sci.* **282,** 1244–1263.
Raiswell R. and Berner R. A. (1985) Pyrite formation in euxinic and semi-euxinic environments. *Amer. J. Sci.* **285,** 710–724.
Raiswell R., Buckley F., Berner R. A., and Anderson T. F. (1988) Degree of pyritization of iron as a paleoenvironmental indicator of bottom-water oxygenation. *J. Sediment. Petrol.* **58,** 812–819.
Raiswell R., Whaler K., Dean S., Coleman M. L., and Briggs D. E. G. (1993) A simple three-dimensional model of diffusion-with-precipitation applied to localised pyrite formation in framboids, fossils and detrital iron minerals. *Mar. Geol.* **113,** 89–100.
Randolf A. D. and Larson M. A. (1988) *Theory of Particulate Processes*. Academic Press.
Rickard D. T. (1970) The origin of framboids. *Lithos* **3,** 269–293.
Roberts A. P. and Turner G. M. (1993) Diagenetic formation of ferrimagnetic iron sulphide minerals in rapidly deposited marine sediments, South Island, New Zealand. *Earth Planet. Sci. Lett.* **115,** 257–273.
Ross D. A. and Degens E. T. (1974) Recent sediments of the Black Sea. In *Black Sea-Geology, Chemistry, and Biology* (ed. E. T. Degens and D. A. Ross); AAPG Mem. 20, pp. 183–199.
Sælen G., Raiswell R., Talbot M. R., Skei J. M., and Bottrell S. H. (1993) Heavy sedimentary sulfur isotopes as indicators of superanoxic bottom-water conditions. *Geology* **21,** 1091–1094.
Sawlowicz Z. (1993) Pyrite framboids and their development: a new conceptual mechanism. *Geol. Rundsch.* **82,** 148–156.
Schallreuter R. (1984) Framboidal pyrite in deep sea sediments. *Initial Rep. Deep Sea Drill. Proj.* **75,** 875–891.
Schoonen M. A. A. and Barnes H. L. (1991) Reactions forming pyrite: I. Nucleation of FeS_2 below 100°C. *Geochim. Cosmochim. Acta* **55,** 1495–1504.
Skei J. (1983) Geochemical and sedimentological considerations of a permanently anoxic fjord-Framvaren, south Norway. *Sediment. Geol.* **36,** 131–145.
Skei J. M. (1988) Formation of framboidal iron sulfide in the water of a permanently anoxic fjord-Framvaren, south Norway. *Mar. Chem.* **23,** 345–352.
Stumm W. (1992) *Chemistry of the Solid-Water Interface*. Wiley.
Suits N. S., Arthur M. A., and Dean W. E. (1993) C-S-Fe systematics in Peru margin muds. *Geol. Soc. Amer. Abstr. Prog.* **25,** A199 (abstr.).

Swain D. J. (1986) The rapid weathering of a siltstone. *J. Proc. Roy. Soc. New South Wales,* **119,** 83–88.

Sweeney R. E. and Kaplan I. R. (1973) Pyrite framboid formation: laboratory synthesis and marine sediments. *Econ. Geol.* **68,** 618–634.

Taylor G. R. (1982) A mechanism for framboid formation as illustrated by a volcanic exhalative sediment. *Mineral. Deposita* **17,** 23–36.

Uyeda N., Nishino M., and Suito E. (1973) Nucleus interaction and fine structures of colloidal gold particles. *J. Colloid Interface Sci.* **43,** 264–276.

Vallentyne J. R. (1963) Isolation of pyrite spherules from recent sediments. *Limnol. Oceanogr.* **8,** 16–30.

Wada H. (1977) The synthesis of greigite from a polysulfide solution at about 100°C. *Bull. Chem. Soc. Japan* **50,** 2615–2617.

White T. S., Morrison J. L., and Kump L. R. (1990) Formation of iron sulfides in modern salt marsh sediments (Wallops Island, Virginia). In *Geochemistry of Sulfur in Fossil Fuels* (ed. W. L. Orr and C. M. White); ACS Symp. Series 429, pp. 204–217.

Wilkin R. T. (1995) Size distribution in sediments, synthesis, and formation mechanism of framboidal pyrite. Ph.D. dissertation, The Pennsylvania State Univ.

Wilkin R. T. and Barnes H. L. (1994) The size distribution of framboidal pyrite: An indicator of bottom-water redox conditions. *Geol. Soc. Amer. Abstr. Prog.* **26,** A353 (abstr.).